GENERATION OF MICROBUBBLES BY SUBCOOLED BOILING OF WATER WITH DISSOLVED INCONDENSABLE GASES

Li, Yuegui ; Hosokawa, Shigeo ; Hayashi, Kosuke ; Tomiyama, Akio ; Shibata, Naoki ; Maeda, Yasunari

(Citation)
Multiphase Science and Technology,33(3):17-31

(Issue Date)
2021

(Resource Type)
journal article

(Version)
Accepted Manuscript

Generation of Micro-Bubbles by Subcooled Boiling of Water with Dissolved Incondensable Gases

Yuegui Li[a], Shigeo Hosokawa[b]*, Kosuke Hayashi[a], Akio Tomiyama[a], Naoki Shibata[c], Yasunari Maeda[c]

[a] Department of Mechanical Engineering, Graduate School Engineering, Kobe University, 1-1 Rokkodai, Nada, Kobe 657-8501, Japan

[b] Faculty of Societal Safety Science, Kansai University, 7-1 Hakubai, Takatsuki, Osaka 569-1098, Japan

[c] Housing Systems Business Group, Panasonic Corporation, 1048 Kadoma, Osaka 571-8686, Japan

Abstract

A compact and efficient micro-bubble generation method based on subcooled boiling on a thin metal wire is proposed in this study. The generation process of micro-bubbles was observed using a high-speed camera to evaluate the bubble diameter and the number density. The experiments were conducted using resistance heating by DC and AC (60Hz) in several electric power conditions. The dependence of the bubble number density on the concentration of the dissolved oxygen implies that micro-bubbles consist of incondensable gases transferred from the liquid phase into vapor bubbles during the bubble generation and growth in boiling and remained in the bubbles during the subsequent condensation. The cyclic heating with AC is more effective for generating micro-bubbles than the constant heating with DC. The number density increases with increasing the time-averaged heat flux, which also increases the mean bubble diameter though the increasing rate of the diameter is not significant.

Keywords: Micro-bubbles, Bubble generation, Bubble number density, Subcooled boiling, Resistance heating

1. Introduction

Micro-bubbles are bubbles less than several hundred microns in diameter and have been named fine-bubbles by the ISO in recent years. Owing to their small sizes, micro-bubbles have a long residence time in the liquid phase and a large gas-liquid interfacial area per unit volume, which promotes physicochemical phenomena such as absorption[1-2]. Micro-bubbles are therefore in use in many fields such as chemistry[3], agriculture[4], medical[5], water treatment[6] and washing process[7], and they are utilized to improve the efficiency and performance of various industrial systems. It is also desired to improve the efficiency of the micro-bubble generation method to further expand the application range of micro-bubbles.

Various micro-bubble generation methods have been proposed so far, e.g. the gas-liquid shearing/Venturi tube (bubble breakup) method[8],[9], the ultrasonic wave bubble generator[10], the method based on stream condensation[11] and the pressurized dissolution method[12-13]. Most of the available methods however require a fluid flow typically with high velocity, a large equipment and a high operating cost. Therefore it is desired to develop a low-cost and compact micro-bubble generator which does not require the fluid flow. Since the bubble generation mechanism of the pressurized dissolution method is not based on effervescent but on shrink of the cavitation bubbles[12], subcooled boiling might be one of the candidates of the micro-bubble generation method.

In this study, we propose a micro-bubble generation method based on subcooled boiling on a heated surface in a liquid with dissolved incondensable gases. Vapor bubbles are generated due to boiling, and they shrink to form micro-bubbles of the incondensable gases after the subsequent condensation. Since the proposed method requires neither a pump nor a complex piping system, it is possible to generate bubbles in a stagnant liquid pool. The position, shape and number of heating surfaces can be changed depending on the application. The advantage of the proposed method is generation of micro-bubbles in arbitrary local positions without liquid supply, so that it can be used in many industrial applications such as water purification

systems and chemical processes without water dilution and circulation as well as milli and micro channel applications. Although the proposed method requires heat input, it can minimize the energy input because it can generate micro-bubbles in any position required. It, therefore, has a potential to contribute to the miniaturization and cost reduction of micro-bubble generation apparatus. We measured the diameter and the number density of generated bubbles to demonstrate the performance of the proposed method.

2. Experimental apparatus and methods

Fig. 1 shows the experimental apparatus, which mainly consisted of the heating thin metal wire, the power source and the water tank. The wire was platinum (Nilako, PT-351165) of 0.10 mm diameter and 30 mm length and was soldered with lead wires. The wire was scrubbed by a sandpaper (#1000) to make small cavities on the surface. The aluminum frame was equipped in the water tank of 80 × 160 × 120 mm^3 in width, depth and height for fixing the platinum wire. The tank was filled with purified water using a water purification device (Millipore, Elix3). The electrical conductivity of the purified water was 6.7×10^{-6} S/m. The amount of water was 1.0×10^{-3} m^3, so that the level of the free surface was 80 mm. The platinum wire was heated by applying a voltage to it for vapor bubble generation. The power supply system was used as the source of AC power (NF ELECTRONIC INSTRUMENTS, 4210 P-STATION MINI) and DC power (ALINCO, DM130MV). The applied voltage was recorded by the data logger (GRAPHTEC, midi LOGGER GL900).

The water temperature T [℃] and the dissolved oxygen concentration DO [kg/m^3] in the water tank were measured using a thermometer and a fluorescent dissolved oxygen concentration meter, respectively. The temperature was initially set at $T = 298 \pm 0.5$ K and DO of purified water was $(8.5 \pm 0.3) \times 10^{-3}$ kg/m^3. Experiments in reduced DO conditions (4.5×10^{-3} and 0.05×10^{-3} kg/m^3) were also conducted to investigate the effects of DO on the micro-bubble generation process. In the condition of DO = 4.5×10^{-3} kg/m^3, the purified water was

degassed by heating, and then the temperature of the water was reduced to room temperature in an airtight container. In the condition of DO = 0.05×10^{-3} kg/m^3, 0.32 kg/m^3 of sodium sulfite was added to water degassed by boiling to further reduce DO by the reaction:

$$2Na_2SO_3 + O_2 \rightarrow 2Na_2SO_4 \quad (1)$$

Note that the incondensable gases other than the oxygen was still dissolved in this condition because only the oxygen was reduced by the chemical reaction. The concentration of Na_2SO_3 is much lower than the concentration in which the effect of Na_2SO_3 on pool boiling heat transfer was reported[14], and therefore, the effect could be negligible in this experiment. The changes in T and DO during the bubble generation experiment is shown in Fig. 2. Although T slightly increases and DO slightly decreases with time due to heating and bubble generation, the changes in T and DO during the measurement time (30 s) were less than 1 % of the initial values.

The bubble generation process was observed using a high-speed video camera (Photron, SA-X2). The imaging area (2.00×2.00 mm^2) was about the central part of the platinum wire as shown in Fig. 3. Since vapor bubbles were detached from the wire and shrunk to the micro-bubbles before they reached 0.15 mm above the wire, the measurement area of 2.00×1.50 mm^2 was set 0.15 mm above the wire. Note that the size of micro-bubbles was little change in the vertical direction in the measurement region, and therefore, the micro-bubbles are in the thermally equilibrium condition.

In the image processing, after detecting the contour of bubbles by the Sobel filter (Fig. 4 (b)) and binarization (Fig. 4 (c)), the geometric centers of bubbles were detected using the normal Hough transform (Fig. 4 (d)). The diameters of the detected bubbles were evaluated as the mean distances between the centers and the contours.

The mean bubble diameter $\bar{d}$ was calculated as

$$\bar{d} = \frac{1}{N}\sum_{i=1}^{N} d_i \quad (2)$$

where d_i is the sphere-volume-equivalent diameter of the ith bubble and N the total number of detected bubbles. The number density $\overline{n_B}$ of micro-bubbles was calculated as

$$\overline{n_B} = \frac{1}{HS}\left[\frac{1}{K}\sum_{j=1}^{K} N_{Bj}\right] \tag{3}$$

where K is the number of sample images (=16,500), H the depth of field (DOF, 570 μm), S the measurement area, and N_{Bj} the number of bubbles in the jth image. The resolution of the captured images was 2 μm/pixel, and therefore, the uncertainty of d is ±2 μm. $\bar{d}$ was calculated from d of over 7 000 bubbles, the uncertainty of $\bar{d}$ is 2.4×10^{-2} μm, which is about 0.2 % of the typical $\bar{d}$. The uncertainty of $\overline{n_B}$ is 4.6×10^{6} m^{-3}, which is about 0.05 % of the typical $\overline{n_B}$.

The mean temperature of the platinum wire is to be proportional to the electric resistance R_P. The temperature of the platinum wire was therefore evaluated from the time-variation of R_P. The magnitude of the difference between the internal temperature and the surface temperature of a cylinder is related to the Biot number B_i. Since B_i (= 0.030) for the present condition was much less than unity, the temperature distribution could be almost uniform on the metal surface, and the temporal change of the temperature was determined only by the relationship between the heat capacity of the wire and the amount of heat transferred through the surface. Therefore, in this study, the heat transfer surface temperature T_W of the platinum wire can be represented by the mean temperature.

3. Results and discussion

3.1. Influence of dissolved oxygen concentration and generation mechanism

We carried out the micro-bubble generation experiments with DO = 8.5×10^{-3}, 4.5×10^{-3} and 0.05×10^{-3} kg/m^3, alternating current of the frequency f = 60 Hz and the time-averaged heat flux $\bar{q}$ = 4.5 MW/m^2. Fig. 5 shows the generation state of micro-bubbles. The number of

micro-bubbles generated at DO = 0.05 × 10^{-3} kg/m^3 was small as shown in Fig. 5 (a) though we could confirm vapor bubbles generated on the platinum wire under this condition as shown in the magnified image, Fig. 5 (d). On the other hand, in Fig. 5 (b), micro-bubbles are more visible at DO = 4.5 × 10^{-3} kg/m^3, and the further increase in DO up to 8.5 × 10^{-3} kg/m^3 (Fig. 5 (c)) results in a large increase in the number of micro-bubbles.

Then, the generation process of individual micro-bubbles was observed using a microscope to confirm the following three generation patterns, A, B and C. An example of the bubble generations in Pattern A is shown in Fig. 6 (a). The vapor bubble grows on the wire surface with volume oscillation by repeating expansion and condensation. The bubble elongates vertically and then detaches from the wire. The second is the process in which only the tip of the vapor bubble is broken off and becomes a micro-bubble when the vapor bubble generated on the platinum wire expands and condenses. Fig. 6 (b) shows a bubble generated in Pattern B. The behavior of the bubble attaching to the wire is similar to that in Pattern A, whereas the micro-bubble is generated by breakup from the parent bubble when the bubble shape becomes unstable due to rapid condensation. Patten C shown in Fig. 6 (c) is very different from the other two; i.e. the vapor bubbles larger than hundred microns collide on the wire, and subsequently they collapse to form multiple micro-bubbles.

The relationship between DO and $\overline{n_B}$ is shown in Fig. 7. $\overline{n_B}$ increases with increasing DO. This is due to the increases in nucleation rate[15],[16] and in active nucleation sites on the wire surface as the concentration of dissolved incondensable gas increases. The number density of 10^{11} m^{-3} is several times larger than that obtained with the pressurized dissolution method [12]. The probability density function (PDF) of the bubble diameter is shown in Fig. 8. The total numbers of samples used in the calculation of PDF were 3.5 × 10^5, 8.9 × 10^4 and 7.4 × 10^4 at DO = 8.5 × 10^{-3}, 4.5 × 10^{-3} and 0.05 × 10^{-3} kg/m^3, respectively. The peak diameter around 10 μm slightly increases and the distribution becomes broader as DO increases, which results in the increase in the mean bubble diameter $\bar{d}$ with increasing DO as shown in Fig. 9. The

nitrogen was also dissolved in the water as well as the oxygen, and the concentration of nitrogen in the saturated condition can be estimated as 14.0×10^{-3} kg/m^3 at 298 K and 9.6×10^{-3} kg/m^3 at 373 K from the Henry's law. The total concentration of the dissolved incondensable gases is estimated as 22.5×10^{-3}, 11.9×10^{-3}, and 9.65×10^{-3} kg/m^3 for DO = 8.5×10^{-3}, 4.5×10^{-3} and 0.05×10^{-3} kg/m^3, respectively. Hence, the small difference in $\overline{n_B}$ between DO = 4.5×10^{-3} and 0.05×10^{-3} kg/m^3 conditions is due to the small difference in the total concentration of dissolved gases.

Based on the dependence of the bubble diameter and the number density on DO, the generation mechanism of micro-bubbles in the subcooled boiling method can be summarized as follows. Vapor bubbles are generated on the heated surface as schematically shown in Fig. 10 (a) when the platinum wire is heated by electric current. In fact, the bubbles consist not only of vapor but also of incondensable gases, e.g., oxygen and nitrogen, coming from the liquid phase during the bubble growth. The bubble size can be as large as several hundred microns at the bubble growth stage (Fig. 5 (d)). Then the bubbles are released from the wire or collapse, and rapidly shrink in the subcooled water due to the condensation of vapor, while the incondensable gases remain inside the bubbles. Thus, micro-bubbles consisting of the incondensable gases appear in the bulk liquid (Fig. 10 (b)). Note that the micro-bubbles contains a very small amount of vapor which is determined by the Dalton's law. When the concentration of the dissolved incondensable gases increases, the number of incondensable gas molecules in the vapor bubbles generated by the heating increases, which results in increase of the number of molecules in the generated micro-bubbles, i.e., the size of the generated micro-bubbles. The number of generated micro-bubbles also increases with the concentration of the dissolved gases due to the increase of bubble nuclei.

3.2. Influence of heat flux with DC and AC

In order to discuss the effects of the heating condition on the micro-bubble generation, $\bar{d}$

and $\overline{n_B}$ of micro-bubbles generated with the electric heating of DC (constant heating) and AC (cyclic heating) (f = 60 Hz) were compared for 1.5 $\leq \bar{q} \leq$ 6.0 MW/m^2. Note that the boiling regime observed was the nucleate boiling in all the conditions. Fig. 11 (a) shows that at $\bar{q}$ = 1.5 MW/m^2, bubbles attaching to the platinum wire grow up to about 0.6 mm diameter and reached the quasi-equilibrium state, while few micro-bubbles are generated for both DC and AC. On the other hand, as shown in Fig. 11 (b)-(d), micro-bubbles are generated for $\bar{q} \geq$ 3.0 MW/m^2, and the amount of bubbles increases as $\bar{q}$ increases. Micro-bubbles were confirmed for $\bar{q} \geq$ 3.0 MW/m^2 in DC and $\bar{q} \geq$ 2.5 MW/m^2 in AC. The reason why the minimum $\bar{q}$ required for micro-bubble generation in AC is slightly lower than in DC is as follows. The wire surface temperature T_w during one cycle and the bubble generation process at $\bar{q}$ = 4.5 MW/m^2 are shown in Fig. 12 and Fig. 13, respectively. Since T_w is constant in the DC case, micro-bubbles were generated from vapor bubbles at a constant generation rate (Fig. 13(a)) and the bubble generation pattern was mainly Patten A (detachment) and B (single breakup) in Fig. 6. On the other hand, the bubble generation rate with AC fluctuates as shown in Fig. 13 (b)-(d), where P_A, P_B and P_C represent the instants shown in Fig. 12. The bubble generation is not observed at the low temperature of P_A (Fig. 13 (b)), while micro-bubbles are generated at P_B, where T_w is higher than the surface temperature with DC and the micro-bubble generation due to bubble collapse (Pattern C in Fig. 6 (c)) is mainly observed. The bubble collapse efficiently produces multiple micro-bubbles, and consequently, the number of micro-bubbles generated with AC is larger than that with DC. As shown in Fig. 11 (c) and (d), the numbers of bubbles on the wire in AC cases are larger than those in DC cases. This implies that the number of active cavities in AC cases are larger than those in DC cases because of the higher maximum heat flux. Thermophoresis of the micro-bubbles toward the wire surface due to high temperature gradient in the vicinity of the wire was also observed during the no bubble generation period in AC cases. The micro-bubbles move to the wire surface and play the role of nuclei in the subsequent boiling period. These are also the reason of high bubble generation rate in AC cases.

Fig. 14 shows the relationship between $\bar{q}$ and $\overline{n_B}$. The $\overline{n_B}$ increases with increasing $\bar{q}$ for both DC and AC. Hence, the $\overline{n_B}$ can be easily controlled by changing electric current. The larger $\overline{n_B}$ with AC implies that AC can generate micro-bubbles more efficiently than DC. The PDFs of the bubble diameter are shown in Fig. 15; the peaks appear around 15 μm for both DC and AC, and the probability around 20-40 μm increases as $\bar{q}$ increases. Fig. 16 shows the relationship between $\bar{q}$ and $\bar{d}$. The $\bar{d}$ slightly increases as $\bar{q}$ increases for both DC and AC, whereas AC gives somewhat larger $\bar{d}$.

3.3. Influence of AC frequency

The f was varied in the range of $15 \leq f \leq 960$ Hz to investigate the influence of f on the micro-bubble generation in the cyclic heating. The $\bar{q}$ was fixed at 4.5 MW/m^2. Fig. 17 shows the state of micro-bubbles generation at time t = 30 s after heating started. The number of bubbles with large diameters decreases as f increases as can also be confirmed in Fig. 18. Fig. 19 shows the relationship between f and $\overline{n_B}$. Though the large f can decrease $\bar{d}$, $\overline{n_B}$ is deteriorated as f increases; the reduction in $\bar{n}_B$ is about 40% by the increase in f from 60 to 240 Hz. Both $\bar{d}$ and $\overline{n_B}$ approach those values in the DC case as f increases.

3.4. Micro-bubble generation using a nichrome wire

Since nichrome wires are often used as a heating element, the performance of the bubble generation method with a nichrome wire was also examined. The nichrome wire (Nilaco, 691167) of 0.10 mm diameter and 30 mm length was used, which was preliminary heated once for a sufficient time to form an oxide film to promote the detachment of micro-bubbles from the wire. The $\bar{q}$ was 4.5 MW/m^2 and 6.0 MW/m^2. The power supply was AC. Fig. 20 shows the state of micro-bubble generation captured at t = 30 s. The micro-bubbles can be generated by the nichrome wire and the generated bubbles are relatively larger than those generated by the platinum wire. The effects of $\bar{q}$ on $\bar{d}$ and $\overline{n_B}$ are shown in Table 1. Being similar to the cases with the platinum wire, $\bar{d}$ and $\overline{n_B}$ obtained with the nichrome wire increase with

increasing $\bar{q}$. At the same $\bar{q}$, $\bar{d}$ is no significant difference between the platinum and nichrome wires, but $\overline{n_B}$ is lower for the nichrome wire. These differences can be attributed to the difference in the surface structure, i.e., the size and number of cavities made by scrubbing by the sandpaper and surface oxidization.

4. Conclusions

The feasibility of micro-bubble generation using subcooled boiling with an electrically heated thin wire was confirmed and the diameter and number density of generated micro-bubbles were measured from high-speed video images. As a result, the following results were obtained:

(1) The proposed method can generate micro-bubbles at a high number density. The dependence of the bubble number density on the concentration of the dissolved oxygen implies that micro-bubbles consist of incondensable gases transferred from the liquid phase into vapor bubbles during the bubble growth in boiling and the subsequent condensation.

(2) The cyclic heating with AC is more effective for generating micro-bubbles than the constant heating with DC.

(3) The number density increases with increasing the time-averaged heat flux, which also increases the mean bubble diameter though the increasing rate of the diameter is not significant.

(4) Both platinum and nichrome wires can be used for the proposed method. The effects of the heat flux on the bubble size and number density are qualitatively the same for both materials.

Acknowledgements

The authors gratefully acknowledge Mr. Masataka Yoshida and Mr. Naoya Iwamoto for their efforts in the experiments.

References

[1] M. Takahashi, T. Kawamura, Y. Yamamoto, H. Ohnari, S. Himuro, H. Shakutsui, Effect of Shrinking Microbubble on Gas Hydrate Formation, J. Phys. Chem. B107 (10) (2003) 2171-2173.

[2] M. Takahashi, ζ Potential of Microbubbles in Aqueous Solutions: Electrical Properties of the Gas−Water Interface, J. Phys. Chem. B 109 (46) (2005) 21858-21864.

[3] M. Matsumoto, T. Fukunaga, K. Onoe, Polymorph control of calcium carbonate by reactive crystallization using microbubble technique, Chem. Eng. Res. Des. 88 (2010) 1624-1630.

[4] Yaxin Liu, Yunpeng Zhou, Tianze Wang, Jiachong Pan, Bo Zhou, Tahir Muhammad, Chunfa Zhou, Yunkai Li, Micro-nano bubble water oxygation: Synergistically improving irrigation water use efficiency, crop yield and quality, J. Cle. Prod. 222 (10) (2019), 835-843.

[5] Y. Kaneko, T. Maruyama, K. Takegami, T. Watanabe, H. Mitsui, K. Hanajiri, H. Nagawa, Y. Matsumoto, Use of a microbubble agent to increase the effects of high intensity focused ultrasound on liver tissue, Eur. Radiol. 15, (2005) 1415-1420.

[6] Li-Bing Chu, Xin-Hui Xing, An-FengYu, Xu-Lin Sun, Benjamin Jurcik, Enhanced treatment of practical textile wastewater by microbubble ozonation, Process Saf. Environ. Protect. 86 (5) (2008), 389-393.

[7] C. Oliveira, R. T. Rodrigues, J. Rubi, A new technique for characterizing aerated flocs in a flocculation – microbubble flotation system, Int. J. Miner. Process. 96 (2009) 36-44.

[8] M. Sadatomi, A. Kawahara, K. Kano, A. Ohtomo, Performance of a new micro- bubble generator with a spherical body in a flowing water tube, Exp. Thermal Fluid Sci. 29 (2005) 615–623.

[9] A. Fujiwara, S. Takagi, K. Watanabe, Y. Matsumoto, Experimental study on the new micro-bubble generator and its application to water purification system, in: Proc. ASME/JSME 2003 4th Joint Fluids Summer Engineering Conference, FEDSM2003-45162, 2003, pp.

469–473.

[10] T. Makuta, F. Takemura, E. Hihara, Y. Matsumoto, M. Shoji, Generation of micro gas bubbles of uniform diameter in an ultrasonic field, J. Fluid Mech. 548 (2006) 113–131.

[11] A. Thiemann, T. Nowak, R. Mettin, F. Holsteyns, A. Lippert, Characterization of an acoustic cavitation bubble structure at 230 kHz, Ultrason. Sonochem. 18 (2) (2011) 595-600.

[12] Y. Maeda , S. Hosokawa , Y. Baba, A. Tomiyama, Y. Ito, Generation mechanism of micro-bubbles in a pressurized dissolution method, Exp. Thermal Fluid Sci. 60 (2015) 201-207

[13] S. Hosokawa, K. Tanaka, Y. Maeda, A. Tomiyama, A. Yamaguchi, Y. Ito, Effect of entrained air bubbles generated by a pressurized dissolution method, Trans. JSME, B 76 (765) (2010) 53–60.

[14] M. Jamialahmadi, A. Helalizadeh, H. M€uller-Steinhagen, Pool boiling heat transfer to electrolyte solutions, International Journal of Heat and Mass Transfer 47, 2004, 729 – 742.

[15] S.D. Lubetkin, Why is it much easier to nucleate gas bubbles than theory predicts?, Langmuir 19 (7) (2003) 2575–2587.

[16] Y. Mori, K. Hijikata, T. Nagatani, Effect of dissolved gas on bubble nucleation, Int. J. Heat Mass Trans. 19 (10) (1976) 1153–1159.

Figure captions

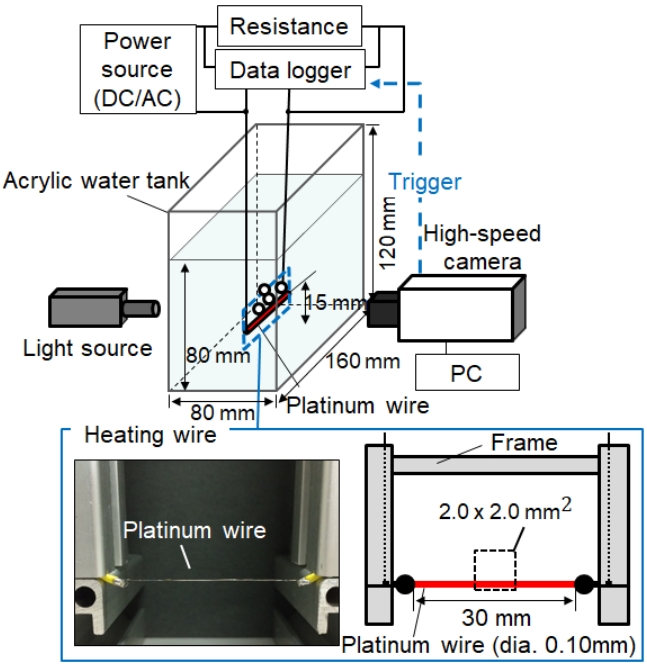

Fig. 1 Experimental apparatus

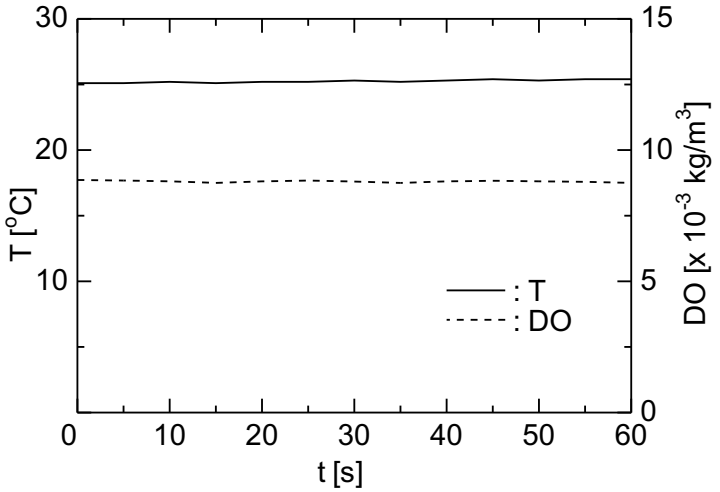

Fig. 2 Changes in *T* and DO

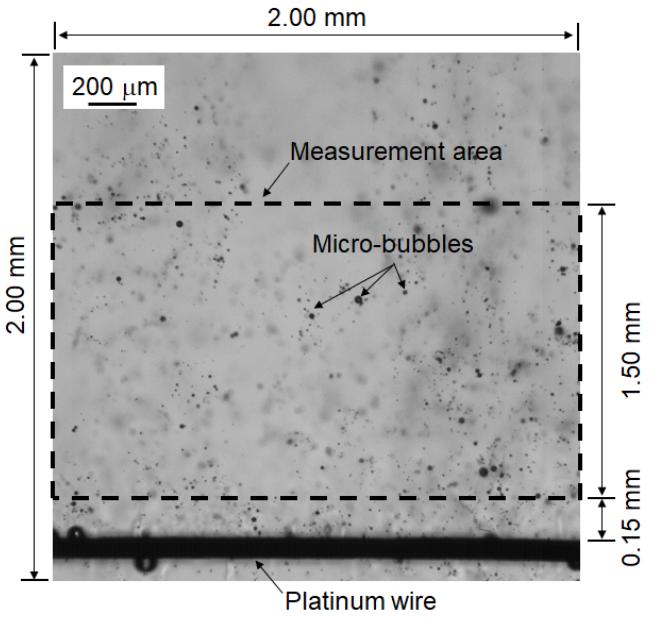

Fig. 3 Imaging area and measurement area

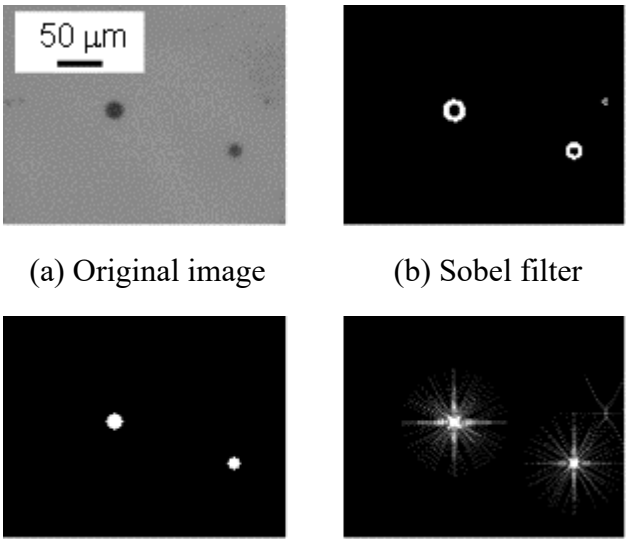

(a) Original image (b) Sobel filter

(c) Binary image (d) Normal Hough transform

Fig. 4 Image processing

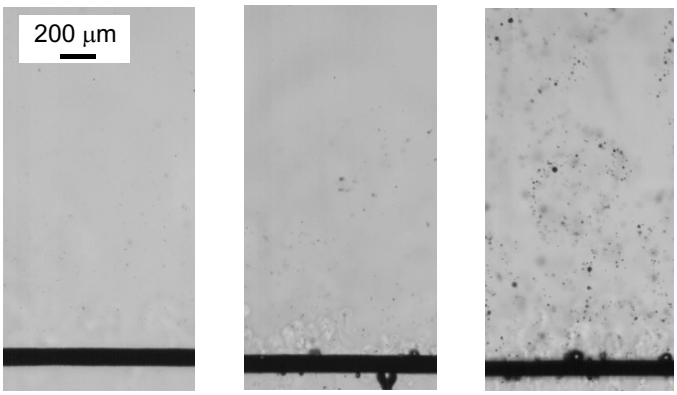

(a) DO = 0.05 **(b)** 4.5 **(c)** 8.5

(x 10^{-3} kg/m^3)

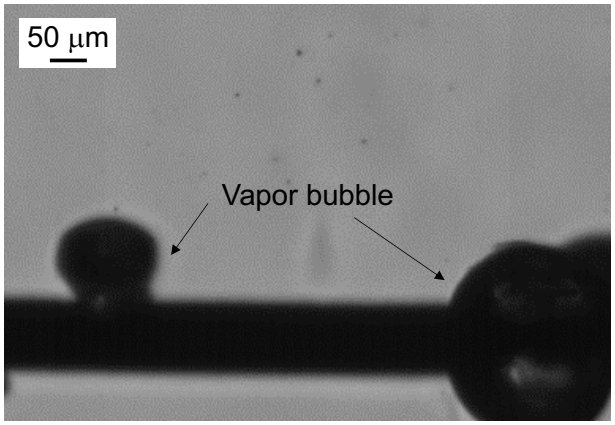

(d) Vapor bubble (DO = 0.05x10^{-3} kg/m^3)

Fig. 5 Images of generated micro-bubbles

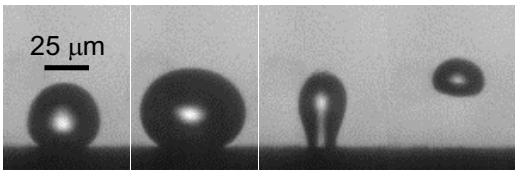

$t = t_0+$

0.0 1.0 3.0 10

x10^{-5}s

(a) Detachment of micro-bubble; Pattern A

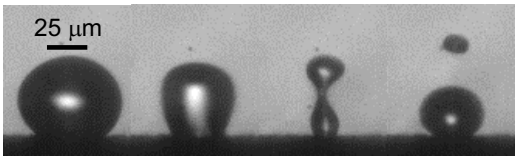

$t = t_0+$

0.0 0.5 1.0 1.5

x10^{-5}s

(b) Break off of vapor bubble; Pattern B

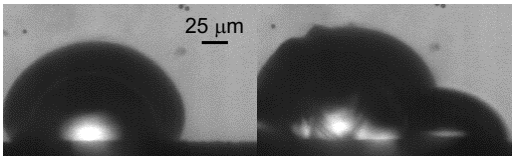

$t = t_0+$

0.0 2.0

x10^{-5}s

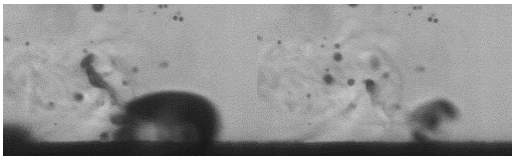

$t = t_0+$

4.0 4.5

x10^{-5}s

(c) Collapses of vapor bubble; Pattern C

Fig. 6 Process of micro-bubble generation

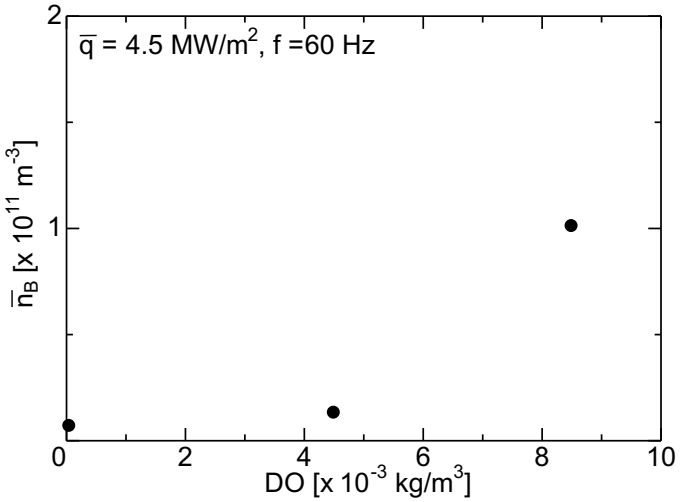

Fig. 7 Effect of DO on $\overline{n_B}$

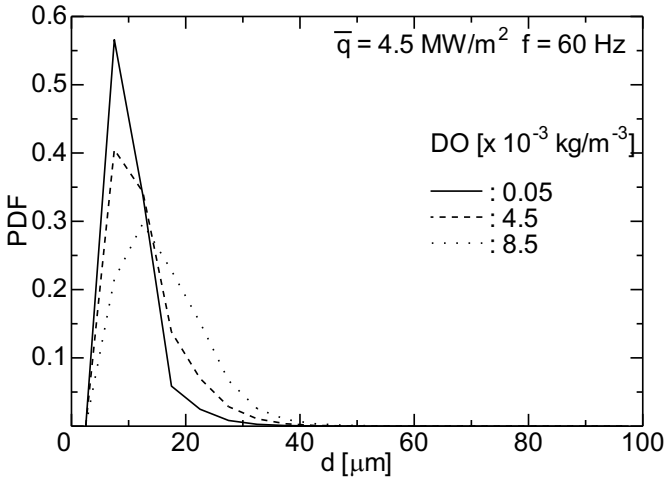

Fig. 8 Bubble size distribution

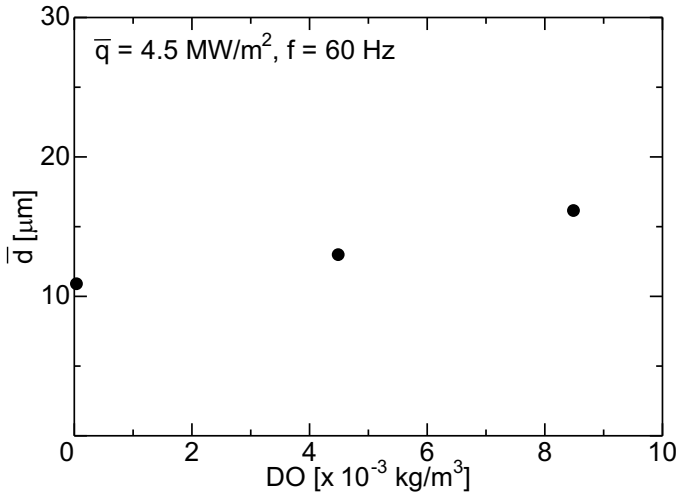

Fig. 9 Effect of DO on $\bar{d}$

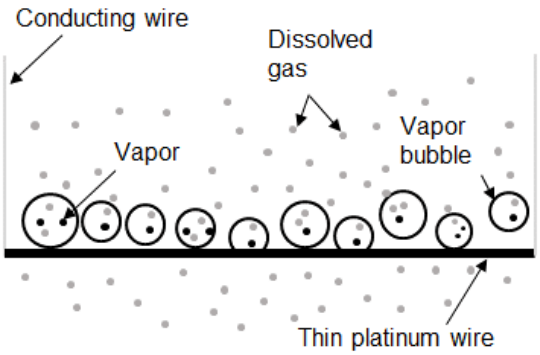

(a) Vapor bubble generation

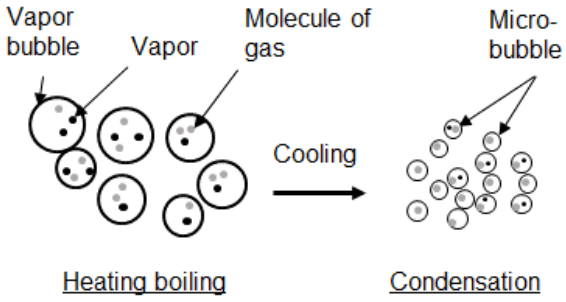

(b) Micro-bubbles consisting of incondensable gases

Fig. 10 Micro-bubble generation process

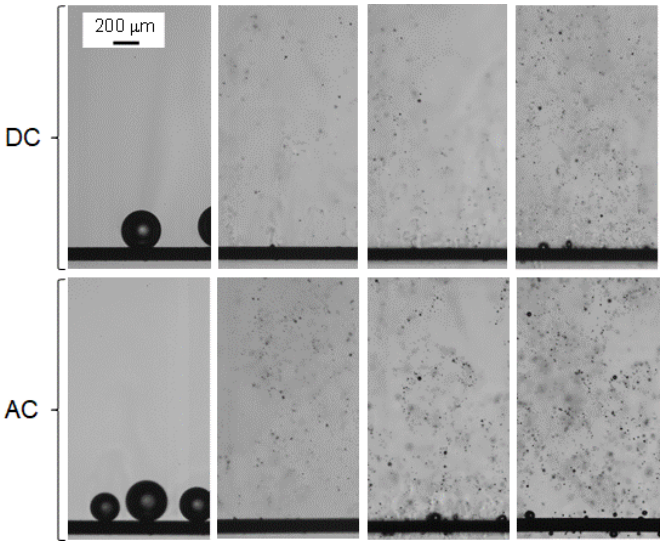

(a) $\bar{q}$ = 1.5 **(b)** 3.0 **(c)** 4.5 **(d)** 6.0

(MW/m^2)

Fig. 11 Images of generated micro-bubbles (Top: DC, Bottom: AC)

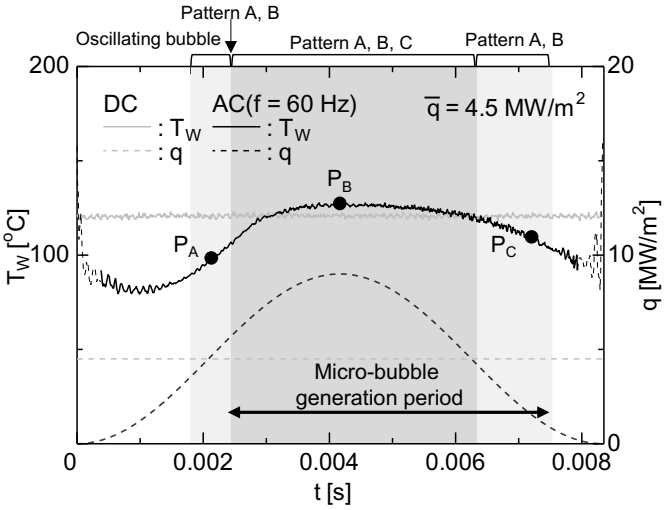

Fig. 12 Heat transfer surface temperature during one cycle ($\overline{q}$ = 4.5 MW/m^2)

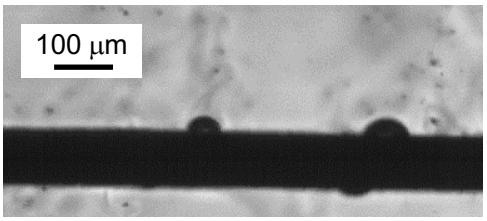

(a) DC

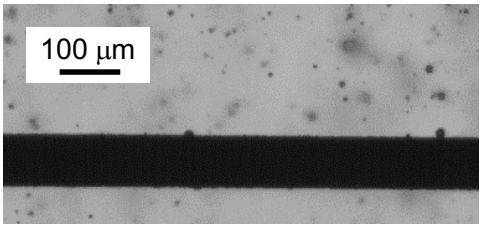

(b) AC t = 0.002 s (P_A)

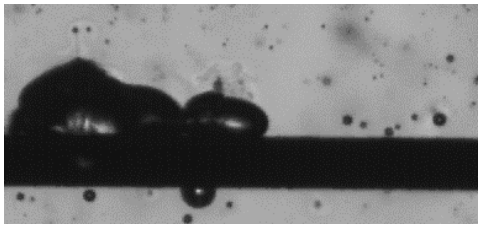

(c) AC t = 0.004 s (P_B)

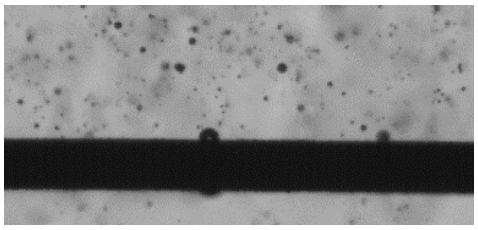

(d) AC t = 0.007 s (P_C)

Fig. 13 Generation state with different heat transfer surface temperature

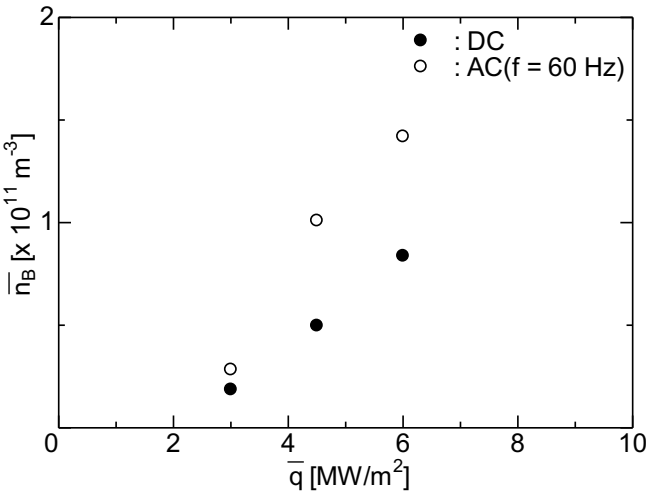

Fig. 14 Effects of $\bar{q}$ on $\overline{n_B}$

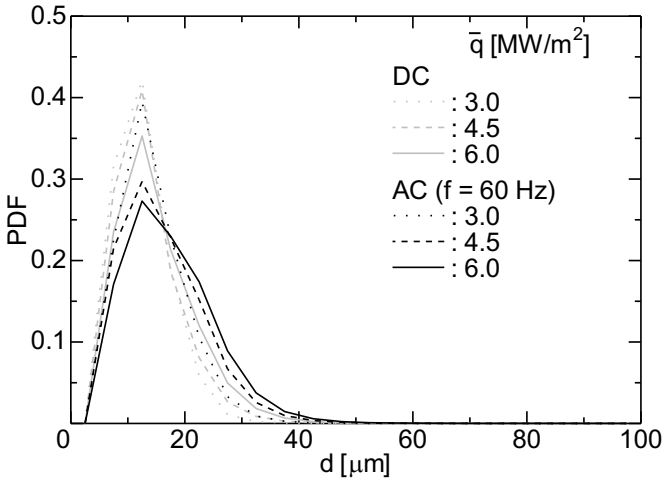

Fig. 15 Bubble size distribution

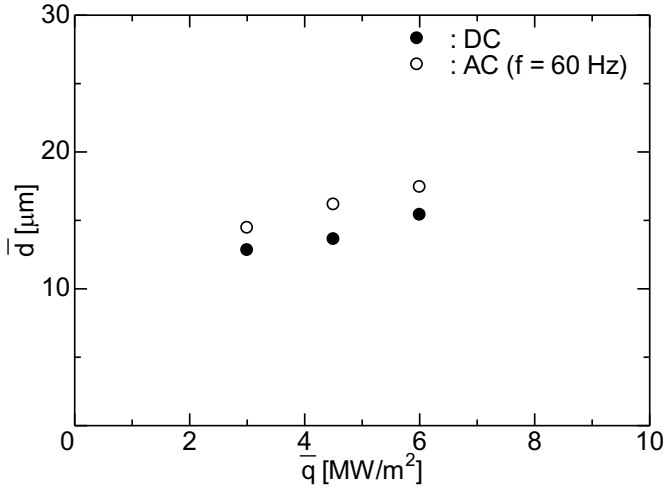

Fig. 16 Effects of $\bar{q}$ on $\bar{d}$

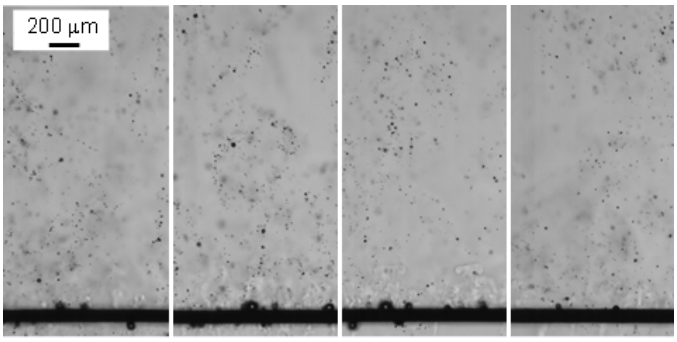

Fig. 17 Micro-bubbles generated with different AC frequencies

(AC, $\bar{q}$ = 4.5 MW/m^2)

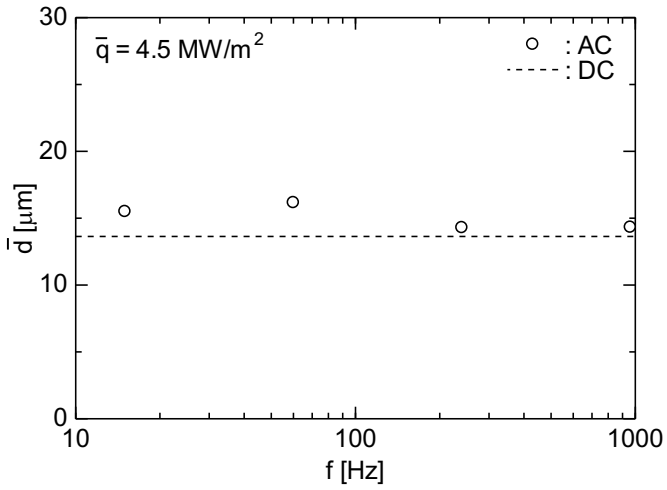

Fig. 18 Relation between f and $\bar{d}$

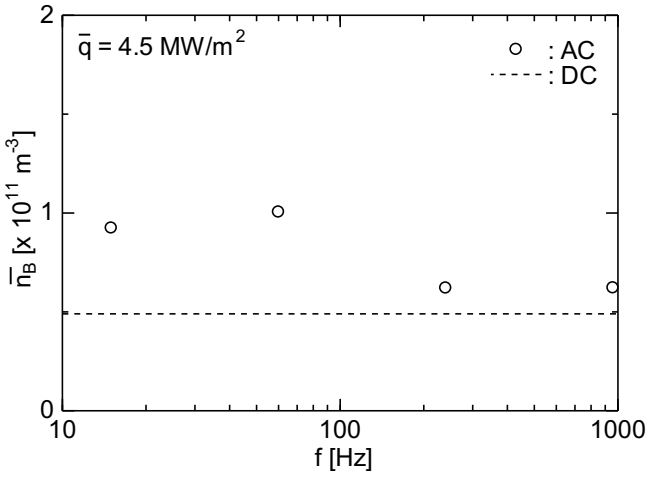

Fig. 19 Relation between f and $\overline{n_B}$

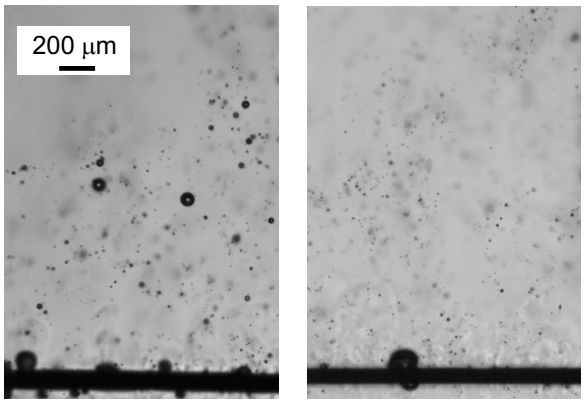

(1) Nichrome wire **(2)** Platinum wire

(a) $\bar{q}$ = 4.5 MW/m^2

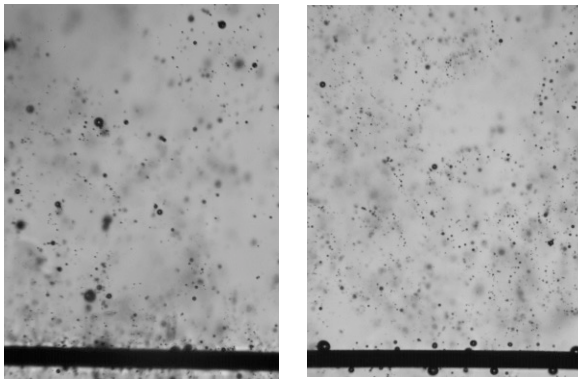

(1) Nichrome wire **(2)** Platinum wire

(b) $\bar{q}$ = 6.0 MW/m^2

Fig. 20 Comparison in bubble generation state between nichrome and platinum wires

Table 1 Relation between $\bar{q}$ and $\bar{d}$ with $\overline{n_B}$

AC, f = 60 Hz	$\bar{q}$ [MW/m^2]	3.0	4.5	6.0
$\bar{d}$ [μm]	platinum wire	14	16	17
	nichrome wire	—	17	18
$\overline{n_B}$ [x10^{11} m^{-3}]	platinum wire	0.28	1.01	1.42
	nichrome wire	—	0.52	0.71